Journal of Sound and Vibration (1998) **216**(3), 413–434
Article No. sv981737

BOUNDARY ELEMENT METHOD FOR ACOUSTIC SCATTERING IN FLUID–FLUIDLIKE AND FLUID–SOLID PROBLEMS

V. Mallardo

Dipartimento di Scienza delle Costruzioni, *Università degli Studi di Napoli*, *Napoli* 80125, *Italy*

AND

M. H. Aliabadi

Department of Engineering, *Queen Mary & Westfield College*, *University of London*, *London E*1 4*NS*, *England*

(*Received* 4 *October* 1996, *and in final form* 20 *April* 1998)

In this paper the application of the two-dimensional boundary element method to the scattering of plane sound waves from an infinite cylinder in a fluid is presented. The acoustic equation of the wave motion in a barotropic, inviscid fluid is deduced from the linearized hydrodynamics equations and the linearized equation of state, while the wave motion inside the solid is described by two different models. Two sets of boundary integral equations are presented for modelling the interaction of fluid–fluidlike and fluid–solid problems. Several test examples are presented to demonstrate the accuracy of the proposed formulations. Comparison with available analytical results, as well as numerical results for different sizes and positions of the internal boundary are given. Farfield coefficients and the results of the scattering cross-section demonstrate the different behaviour of the two models and the influence of the internal boundary.

1. INTRODUCTION

Scattering of acoustic and electromagnetic waves are important in many engineering fields such as mechanics and aeronautics among others. It can give important information about the internal composition of solids and fluids. For example, in non-destructive testing one can obtain information about internal inhomogeneities, non-symmetries and defects from the scattering pattern.

There are several applications of the finite element method to scattering problems and in particular electromagnetic scattering. To overcome the inability to deal with open field scattering problems, the finite element method has always been coupled with analytic or other numerical methods, for example, with the bymoment method [1], modal expansion [2], adsorbing boundary condition [3, 4], and boundary integral equations [5, 8].

0022–460X/98/380413 + 22 $30.00/0

The boundary element method has been successfully applied in many problems involving infinite domains [9–12]. Its important advantages are that the solution space is one dimension lower than that of the geometry, and that the Green's function-based integral kernels implicitly assure the satisfaction of the Sommerfield radiation condition. Contributions to the acoustic scattering problem in the case of an impenetrable obstacle can be found in references [13–17].

Acoustic scattering with coupling conditions on the interface has been solved in 3-D by Seybert *et al*. [18, 19], Goswami *et al*. [20] but no applications in 2-D have been reported.

In this paper, the two-dimensional boundary element method is applied for the first time to solve the coupled problem for two different types of obstacle. In both cases an acoustic incident incoming wave is scattered by an obstacle. The main difference between the 2-D and 3-D applications, apart from the discretization procedures, is the complexity of the fundamental solutions in the two-dimensional problem.

In the first part, the obstacle is modelled by the Helmholtz equation as a fluid, i.e., it is not able to support shear waves. The external and internal scalar fields are coupled on the interface by their respective pressures and fluxes.

In the second part, the scatterer's field is governed by the Navier–Cauchy equation, i.e., longitudinal and transverse waves are present inside, with displacements and tractions coupled on the interface with the external scalar quantities.

To demonstrate the efficiency of the method, numerical examples are presented for a configuration for which any analytical solution is available.

In order to compare the results of the two models, the examples refer to the same scatterer (brass). It has to be pointed out that the first model does not describe in a physically efficient way the scatterer whose transverse wave velocity is comparable to the longitudinal wave velocity. However, it can be used for materials, like rubber, characterised by the low value of the Lamé constant μ and, of course, for fluid.

2. FLUID–FLUIDLIKE SCATTERING

2.1. THE INTERACTION MODEL

The model consists of the coupling of two sets of integral equations which represent respectively the response of an obstacle and the acoustic behavior of the fluid in the presence of an incident beam. The two equations are coupled by enforcing continuity of normal components of velocities and equilibrium of pressures along the interface. The obstacle response is characterised by the internal pressure p_i, while the external behaviour is characterised by the total pressure p_e. The total pressure is taken as the sum of the incident p_{inc} and scattered p_{sc} pressure, i.e.,

$$p_e(\mathbf{x}) = p_{inc}(\mathbf{x}) + p_{sc}(\mathbf{x}).$$

The scattered pressure p_{sc} satisfies the Sommerfield radiation condition at infinity [21].

Consider the problem shown in Figure 1, where Ω_e is the exterior medium carrying the incident beam $p_{inc}(\mathbf{x})$, Ω_i is the interior domain with the cavity, Γ_e is the interface between Ω_e and Ω_i, and Γ_i is the internal boundary.

Considering time-harmonic analysis, the variation $\exp(-i\omega t)$ is assumed for all the field variables, with ω being the circular frequency ($\omega = 2\pi f$) in radians per second, $i = \sqrt{-1}$ and t is the time. For this linear steady state problem, p_i, p_{inc}, and p_{sc} all satisfy the Helmholtz wave equation, that is

$$\Delta^2 p(\mathbf{x}) + k^2 p(\mathbf{x}) = 0, \tag{1}$$

$$k = k_e \quad \text{for} \quad x \in \Omega_e, \qquad k = k_i \quad \text{for} \quad x \in \Omega_i,$$

where k_e and k_i are the external and internal wave numbers, respectively. They are given as

$$k_e = \frac{\omega}{c_e} \quad c_e = \text{external wave speed}, \quad k_i = \frac{\omega}{c_i} \quad c_i = \text{internal wave speed}.$$

At the interface Γ_e, the external and internal pressure and flux satisfy the boundary conditions given by

$$p_e(\mathbf{x}) = p_i(\mathbf{x}), \qquad \frac{1}{\rho_e} q_e(\mathbf{x}) = -\frac{1}{\rho_i} q_i(\mathbf{x}), \tag{2}$$

where ρ_e and ρ_i are external and internal densities, respectively. The external and internal fluxes can be defined as

$$q_e(\mathbf{x}) = \frac{\partial p_e(\mathbf{x})}{\partial n_e(\mathbf{x})}, \qquad q_i(\mathbf{x}) = \frac{\partial p_i(\mathbf{x})}{\partial n_i(\mathbf{x})}.$$

On the internal boundary Γ_i one can choose either conditions, that is

$$q(\mathbf{x}) = 0 \quad \text{or} \quad p(\mathbf{x}) = 0. \tag{3}$$

The boundary integral equations corresponding to the field equation (1) can be written as

$$c(\boldsymbol{\xi}) p_e(\boldsymbol{\xi}) + \int_{\Gamma_e} q^*(\boldsymbol{\xi}, \mathbf{x}) p_e(\mathbf{x})\, \mathrm{d}\Gamma_e(\mathbf{x}) = \int_{\Gamma_e} p^*(\boldsymbol{\xi}, \mathbf{x}) q_e(\mathbf{x})\, \mathrm{d}\Gamma_e(\mathbf{x}) + p_{inc}(\boldsymbol{\xi}) \tag{4a}$$

for the exterior problem, and

$$c(\boldsymbol{\xi}) p_i(\boldsymbol{\xi}) + \int_{\Gamma} q^*(\boldsymbol{\xi}, \mathbf{x}) p_i(\mathbf{x})\, \mathrm{d}\Gamma(\mathbf{x}) = \int_{\Gamma} p^*(\boldsymbol{\xi}, \mathbf{x}) q_i(\mathbf{x})\, \mathrm{d}\Gamma(\mathbf{x}) \tag{4b}$$

for the interior problem.

The integral equation (4a) is applied only to the interface Γ_e, while equation (4b) is used for the whole boundary $\Gamma = \Gamma_e \cup \Gamma_i$.

The points ξ, $\mathbf{x}$ are referred to as the source and field points, respectively, r is the modulus of the vector $(\xi - \mathbf{x})$ and $p^*(\xi, \mathbf{x})$, $q^*(\xi, \mathbf{x})$ are the fundamental solutions characterising the response of a point disturbance in an infinite 2-D domain, given as

$$p^*(\xi, \mathbf{x}) = \frac{1}{2\pi} \mathrm{K}_0(\mathrm{i}kr)$$

$$q^*(\xi, \mathbf{x}) = -\frac{\mathrm{i}\pi}{2\pi} \mathrm{K}_1(\mathrm{i}kr) \frac{\partial r}{\partial \mathbf{n}(\mathbf{x})}. \tag{5}$$

The terms K_0 and K_1 are the zero and first order modified Bessel functions of the second kind, respectively.

The coefficient $c(\xi)$ depends on the local geometry of the boundary and is equal to 1/2 for smooth boundaries. The singularities of the fundamental solutions $p(\xi, \mathbf{x})$ and $q(\xi, \mathbf{x})$ are of $O(\ln r)$ and $O(1/r)$, respectively, but the term $\partial r/\partial \mathbf{n}$ smooths the singularity in $\mathrm{K}_1(\mathrm{i}kr)$.

It should be noted that in using formulation (4a), some difficulties can be encountered due to the presence of spurious results if k is near certain characteristic frequencies (see reference [22]). The theory behind this problem is quite complicated. It can be demonstrated that these characteristic frequencies are the resonance frequencies (or the eigenfrequencies) of the auxiliary interior Dirichlet problem.

It has to be pointed out that these frequencies have no physical meaning for the exterior boundary value problem of equation (4a), which has a unique solution for all frequencies. The non-uniqueness is a purely mathematical problem arising from the boundary integral formulation rather than from the nature of the physical problem.

Several modified integral formulations have been proposed to overcome the non-uniqueness problem. The Combined Helmholtz Integral Equation Formulation (CHIEF) proposed by Schenck uses equation (4a) with source points inside the body as a constraint that must be satisifed along with the usual Helmholtz integral equation on the boundary. The resulting overdetermined system may then be solved by a least-square procedure. Another well known formulation is proposed by Burton and Miller [23]. This approach consists of a linear combination of the Helmholtz integral equation and its normal derivative: it has been proved in reference [23] that the linear combination of these two equations will yield a unique solution for all frequencies if the constant multiplying the derivative equation is appropriately chosen. However, the major difficulty in this formulation is that the normal derivative of the Helmholtz integral equation involves a hyper-singular integral. In reference [23], Burton and Miller used a double surface integral to regularise this strong singularity, but evaluation of a double integral is computationally costly. Other regularisation techniques, such as the work by Meyer *et al*. [24] and Terai [12], are valid for planar elements only.

The non-uniqueness problem is outside of the scope of this paper, which is to measure the sensibility of the solution to the presence of an internal flaw and to compare two different models of investigation. Therefore, it is assumed that the

wave number k is far from every eigenfrequency of the interior Dirichlet problem of the scatterer.

2.2. NUMERICAL IMPLEMENTATION

Assuming that the boundary Γ is discretized into $EL = EL_e + EL_i$ elements, the integral representations (4a) and (4b) can be written as

$$c(\bar{\xi})p_e(\bar{\xi}) + \sum_{l=1}^{EL_e} \int_{\Gamma_l} q^*(\bar{\xi}, \mathbf{x})p_e(\mathbf{x})\,\mathrm{d}\Gamma(\mathbf{x}) = \sum_{l=1}^{EL_e} \int_{\Gamma_l} p^*(\bar{\xi}, \mathbf{x})q_e(\mathbf{x})\,\mathrm{d}\Gamma(\mathbf{x}) + p_{inc}(\bar{\xi}), \tag{6a}$$

$$c(\bar{\xi})p_i(\bar{\xi}) + \sum_{l=1}^{EL} \int_{\Gamma_l} q^*(\bar{\xi}, \mathbf{x})p_i(\mathbf{x})\,\mathrm{d}\Gamma = \sum_{l=1}^{EL} \int_{\Gamma_l} p^*(\bar{\xi}, \mathbf{x})q_i(\mathbf{x})\,\mathrm{d}\Gamma. \tag{6b}$$

The Cartesian co-ordinates of points located within each element Γ_l are expressed in terms of shape functions $\phi(\zeta)$ and co-ordinates of nodal points, i.e.,

$$\mathbf{x} = \sum_{n=1}^{N} \phi_n(\zeta)\mathbf{x}_n,$$

where N is the number of points necessary to define the geometry of the element and ζ a dimensionless local co-ordinate varying in $[-1, 1]$. The unknown external and internal pressures and fluxes along the boundary element are also approximated over each element through interpolation functions $\beta(\zeta)$ and their nodal values, in the form:

$$p(\mathbf{x}) = \sum_{n=1}^{M} \phi_n(\zeta)p_n, \qquad q(\mathbf{x}) = \sum_{n=1}^{M} \phi_n(\zeta)q_n,$$

where M is the number of nodal points within the element.

Three types of boundary element are commonly used in 2-D analysis: constant, linear and quadratic. The computer program developed allows for quadratic isoparametric ($\phi_n = \beta_n$) elements. Therefore, equations (6a) and (6b) can be written as

$$c(\bar{\xi})p_e(\bar{\xi}) + \sum_{l=1}^{EL_e} \sum_{n=1}^{3} \left\{ \int_{-1}^{+1} q^*(\bar{\xi}, \mathbf{x}(\zeta))\phi_n(\zeta)J_l(\zeta)\,\mathrm{d}\zeta \right\} p_e^n$$

$$= \sum_{l=1}^{EL_e} \sum_{n=1}^{3} \left\{ \int_{-1}^{+1} p^*(\bar{\xi}, \mathbf{x}(\zeta))\phi_n(\zeta)J_l(\zeta)\,\mathrm{d}\zeta \right\} q_e^n + p_{inc}(\bar{\xi}) \tag{7a}$$

$$c(\bar{\boldsymbol{\xi}})p_i(\bar{\boldsymbol{\xi}}) + \sum_{l=1}^{EL}\sum_{n=1}^{3}\left\{\int_{-1}^{+1} q^*(\bar{\boldsymbol{\xi}}, \mathbf{x}(\zeta))\phi_n(\zeta)J_l(\zeta)\,\mathrm{d}\zeta\right\}p_i^n$$

$$= \sum_{l=1}^{EL}\sum_{n=1}^{3}\left\{\int_{-1}^{+1} p^*(\bar{\boldsymbol{\xi}}, \mathbf{x}(\zeta))\phi_n(\zeta)J_l(\zeta)\,\mathrm{d}\zeta\right\}q_i^n \tag{7b}$$

where $J_l(\zeta)$ is the Jacobian of the transformation and the shape functions are given as:

$$\phi_1(\zeta) = \tfrac{1}{2}\zeta(\zeta - 1) \quad \phi_2(\zeta) = (1 - \zeta)(1 + \zeta) \quad \phi_3(\zeta) = \tfrac{1}{2}\zeta(\zeta + 1).$$

The first equation is applied on the interface Γ_e, the second one on the boundary Γ; the term $c(\boldsymbol{\xi})$ takes the value 1/2 for all the nodes inside the elements, the value $\theta/2\pi$, where θ is the internal angle, for nodes on the extremes.

Equations (7a) and (7b) applied respectively on all nodes of Γ_e and Γ, represent the uncoupled BIEs where the unknowns are external and internal pressures and fluxes. They can be written in matrix form as

$$\mathbf{H}^e\mathbf{p}^e - \mathbf{G}^e\mathbf{q}^e = \mathbf{p}_{inc}, \qquad \mathbf{H}^i\mathbf{p}^i - \mathbf{G}^i\mathbf{q}^i = 0. \tag{8}$$

The vectors $\mathbf{p}^e$, $\mathbf{q}^e$ and $\mathbf{p}^i$, $\mathbf{q}^i$ collect the external and internal pressures and fluxes, respectively.

The determination of these quantities requires a solution of the two discretized sets of integral equations, after enforcing the boundary conditions (2) on Γ_e and (3) on Γ_i.

The final system of equations can be written as

$$\begin{bmatrix} \mathbf{H}^e & \mathbf{0} & \mathbf{0} & -\mathbf{G}^e & \mathbf{0} \\ \mathbf{0} & \mathbf{H}^i_{\Gamma_e\Gamma_e} & \mathbf{H}^i_{\Gamma_e\Gamma_i} & \mathbf{0} & -\mathbf{G}^i_{\Gamma_e\Gamma_e} \\ \mathbf{0} & \mathbf{H}^i_{\Gamma_i\Gamma_e} & \mathbf{H}^i_{\Gamma_i\Gamma_i} & \mathbf{0} & -\mathbf{G}^i_{\Gamma_i\Gamma_e} \\ \mathbf{I} & -\mathbf{I} & \mathbf{0} & \mathbf{0} & \mathbf{0} \\ \mathbf{0} & \mathbf{0} & \dfrac{\mathbf{I}}{\rho_e} & \dfrac{\mathbf{I}}{\rho_i} & \mathbf{0} \end{bmatrix} \begin{Bmatrix} \mathbf{p}^e \\ \mathbf{p}^i_{\Gamma_e} \\ \mathbf{p}^i_{\Gamma_i} \\ \mathbf{q}^e \\ \mathbf{q}^i_{\Gamma_e} \end{Bmatrix} = \begin{Bmatrix} \mathbf{p}_{inc} \\ \mathbf{0} \\ \mathbf{0} \\ \mathbf{0} \\ \mathbf{0} \end{Bmatrix},$$

if $q = 0$ is assumed on Γ_i, and

$$\begin{bmatrix} \mathbf{H}^e & \mathbf{0} & -\mathbf{G}^e & \mathbf{0} & \mathbf{0} \\ \mathbf{0} & \mathbf{H}^i_{\Gamma_e\Gamma_e} & \mathbf{0} & -\mathbf{G}^i_{\Gamma_e\Gamma_e} & -\mathbf{G}^i_{\Gamma_e\Gamma_i} \\ \mathbf{0} & \mathbf{H}^i_{\Gamma_i\Gamma_e} & \mathbf{0} & -\mathbf{G}^i_{\Gamma_i\Gamma_e} & -\mathbf{G}^i_{\Gamma_i\Gamma_i} \\ \mathbf{I} & -\mathbf{I} & \mathbf{0} & \mathbf{0} & \mathbf{0} \\ \mathbf{0} & \mathbf{0} & \dfrac{\mathbf{I}}{\rho_e} & \dfrac{\mathbf{I}}{\rho_i} & \mathbf{0} \end{bmatrix} \begin{Bmatrix} \mathbf{p}^e \\ \mathbf{p}^i_{\Gamma_e} \\ \mathbf{q}^e \\ \mathbf{q}^i_{\Gamma_e} \\ \mathbf{q}^i_{\Gamma_i} \end{Bmatrix} = \begin{Bmatrix} \mathbf{p}_{inc} \\ \mathbf{0} \\ \mathbf{0} \\ \mathbf{0} \\ \mathbf{0} \end{Bmatrix},$$

if $p = 0$ is assumed on Γ_i.

The matrix $\mathbf{H}^i_{SQ}$ is the submatrix of $\mathbf{H}^i$ generated when the source point belongs to the boundary S and the integration element belongs to the boundary Q. The same for the submatrices of $\mathbf{G}^i$.

The Bessel functions involved in the kernels are calculated using two different series expansions [25], one for small arguments and the other for large arguments. The limit between the two ranges is $|z_{lim}| = 5$, i.e., the value of the argument which gives an error of the same magnitude for both expansions. The elements of **H** and **G** are evaluated numerically by Gaussian quadrature with ten points, except when the element contains the collocation point. In this case, following references [26, 27], the fundamental solutions are divided into two parts, the static value and the remaining part up to the dynamic one. In this way only the static part keeps the singularity because the singularities of the static and the dynamic fundamental solutions for $r \to 0$ are the same.

The diagonal term of the **H** matrix is evaluated by applying constant pressure in the static case, taking into account that the coefficients $c(\bar{\xi})$ are the same in statics and dynamics, and that when dealing with the infinite domain Ω_e the integral over the external boundary Γ_∞ at infinity is not zero. The singular term of the **G** matrix can be evaluated numerically using a special type Gaussian integration formula with logarithmic weight function.

2.3. NUMERICAL EXAMPLES

Consider a cylinder with an internal circular cavity, as shown in Figure 2; the dimensions and the properties of the external fluid and those of the scatterer are given in Table 1.

The incident wave considered is plane and is related to the polar co-ordinates (r, θ) of the generic point **x** by the following expression

$$p_{inc}(\mathbf{x}) = p_0 \exp[-\mathrm{i}k_e r \cos(\theta - \alpha_{inc})],$$

where α_{inc} is the angle between the wave direction and the x_1 axis.

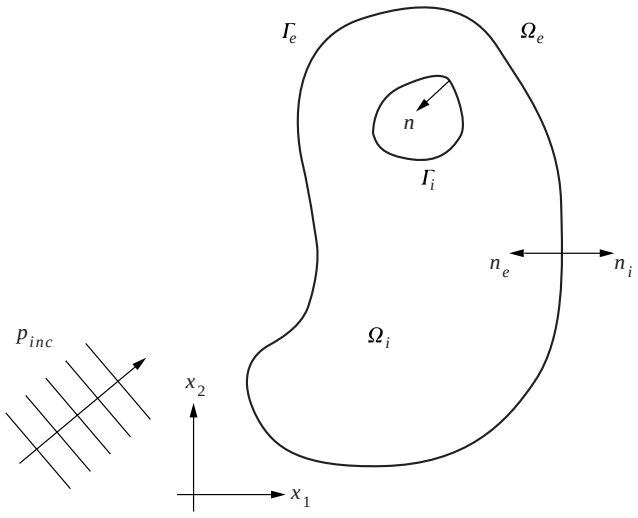

Figure 1. Geometry of the problem.

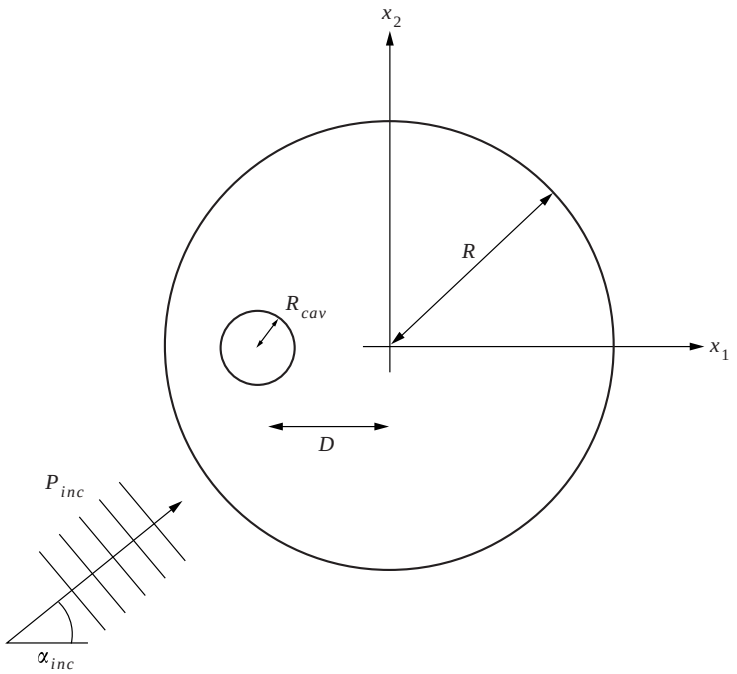

Figure 2. Geometry of the numerical examples.

In order to assess the accuracy of the coupled BEM formulation, two test examples are considered for which analytical solutions are available. Figures 3 and 4 refer to the case of a circular cylinder with an internal central cavity ($R_{cav} = 0{\cdot}05R$) immersed in water and scattering an incident plane wave with direction $\alpha_{inc} = 0^\circ$. These figures compare the analytical and BEM results in the case of $k_eR = 1$ and $k_eR = 10$, for both boundary conditions (3) on Γ_i.

The values reported give the farfield coefficient, defined as:

$$P(\theta) = \left[\frac{\pi k_e r}{2}\right]^{1/2} p_{sc}(r, \theta)\, \mathrm{e}^{\mathrm{i}(\pi/4 - k_e r)}.$$

TABLE 1

Materials properties

Brass cylinder	
Mass density	$\rho = 8500\ \mathrm{kg/m^3}$
Young's modulus	$E = 10{\cdot}5 \cdot 10^{11}\ \mathrm{Pa}$
Poisson's ratio	$v = 1/3$
Radius	$R = 1{\cdot}0\ \mathrm{m}$
Acoustic medium: water	
Mass density	$\rho = 998\ \mathrm{kg/m^3}$
Sound speed	$c = 1486\ \mathrm{m/s}$

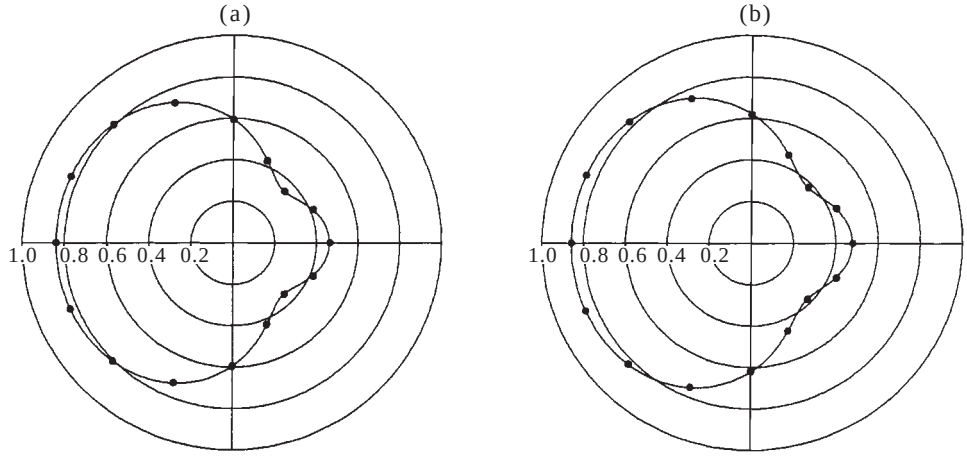

Figure 3. Angular distribution $|p_{sc}/p_{inc}|$ for brass in water with central cavity. Fluidlike scatterer $k_e R = 1$: (a) zero flux on Γ_i; (b) zero pressure on Γ_i. ——, Analytical solution; ●, BEM solution.

normalised to the pressure of the incident wave and the factor $[2/\pi k_e r]^{1/2}$. This coefficient is independent of r for r tending to infinity and is given in terms of the value of the scattered pressure p_{sc}. Its value has been determined at $r = 100R$.

The analytical solution [28] is not available in closed form, but is given in terms of a series expansion in which the mth term involves the Bessel functions of the first kind J_m and of the third kind H_m. In order to obtain a satisfactory stable solution, the first 25 terms of the series solution and 20 terms of the expansion of the Bessel and Hankel functions (see reference [25]) were taken into account.

The tests show that there is a good agreement between the boundary element and the analytical solution. The BEM model consists of eight elements on Γ_e and four on Γ_i in the case $k_e R = 1$, and 28 elements on Γ_e and four elements on Γ_i in the case $k_e R = 10$. These values have been enough to obtain a numerical solution with an error smaller than 1%.

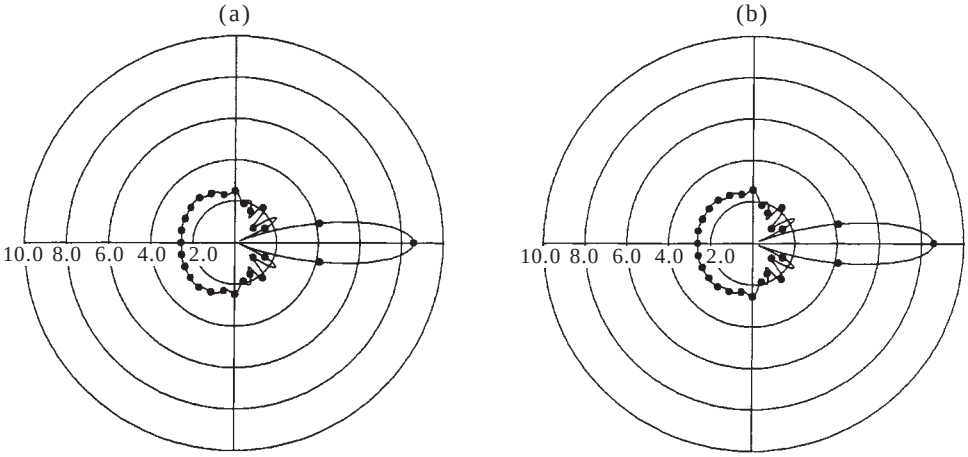

Figure 4. Angular distribution $|p_{sc}/p_{inc}|$ for brass in water with central cavity. Fluidlike scatterer $k_e R = 10$: (a) zero flux on Γ_i; (b) zero pressure on Γ_i. ——, Analytical solution; ●, BEM solution.

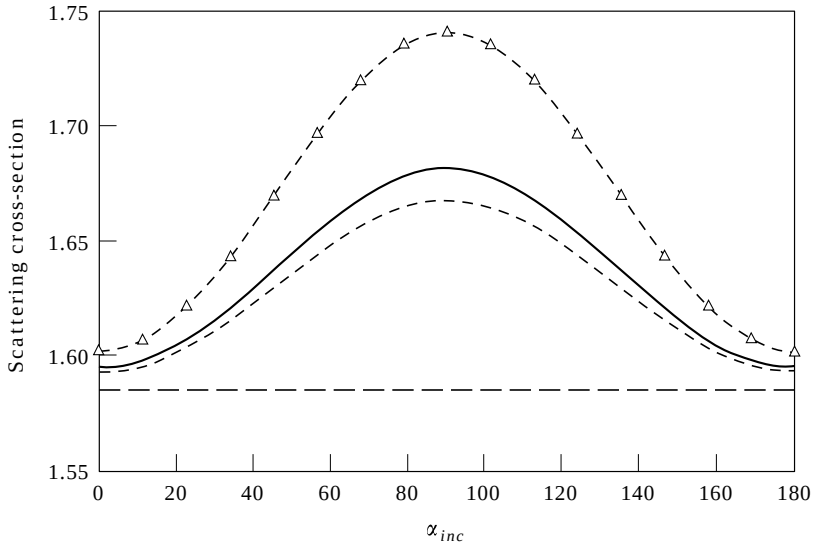

Figure 5. Fluidlike scatterer $k_e R = 1$ and $D = 0{\cdot}6R$. ——, $R_{cav} = 0{\cdot}0R$; – – – –, $R_{cav} = 0{\cdot}05R$; ——, $R_{cav} = 0{\cdot}01R$; –△–△–△–, $R_{cav} = 0{\cdot}005R$.

The higher number of elements in the case $k_e R = 10$ is due to a more unstable solution. Further examples are given in Figures 5–10 where the behaviour of the scattering cross-section (as defined in reference [29]) versus the incident wave's angle, is shown for different dimensionless wave numbers and different sizes and positions of the internal cavity. In all these examples $p = 0$ is the boundary condition considered on Γ_i. The numerical response of the cylinder with internal boundary can be used to characterise the size and position of the cavity.

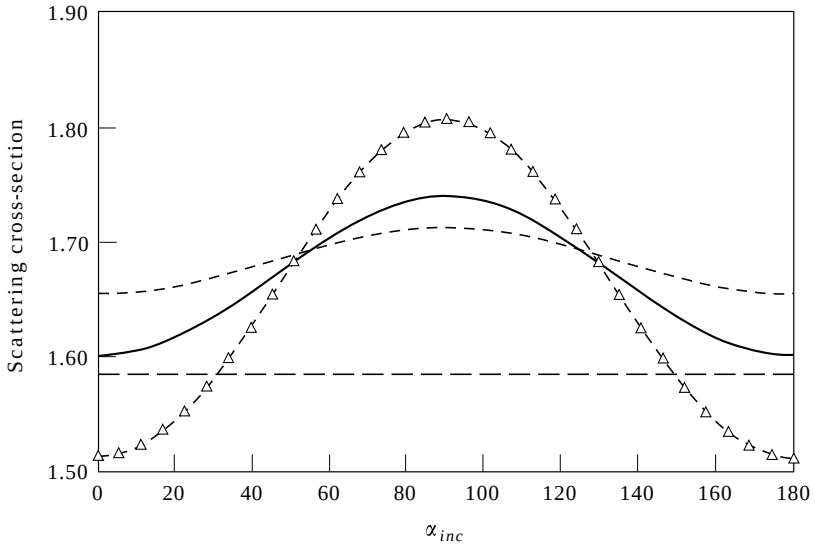

Figure 6. Fluidlike scatterer $k_e R = 1$ and $R_{cav} = 0{\cdot}05R$. ——, $D = 0{\cdot}0R$; – – – –, $D = 0{\cdot}04R$; ——, $D = 0{\cdot}06R$; –△–△–△–, $D = 0{\cdot}8R$.

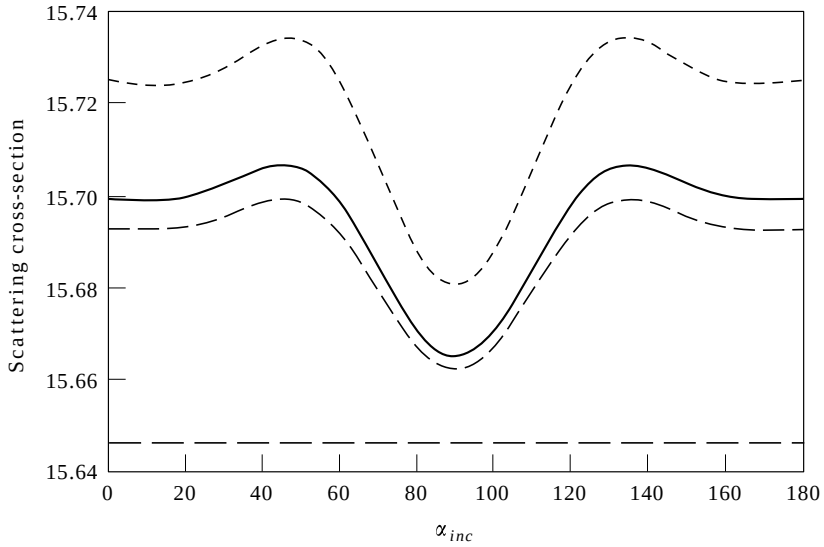

Figure 7. Fluidlike scatterer $k_e R = 5$ and $D = 0{\cdot}6R$. ——, $R_{cav} = 0{\cdot}0R$; – – – –, $R_{cav} = 0{\cdot}005R$; ——, $R_{cav} = 0{\cdot}01R$; ----, $R_{cav} = 0{\cdot}05R$.

In the case of different cavity sizes, increasing the wave number, the incident angle, for which the scattering cross-section presents the maximum difference between the solid with a cavity and the solid without a cavity, moves from 90° towards 0°. The shape of the diagram is not influenced by the size of the cavity.

The scattering cross-section percentage difference between solid with cavity and solid without cavity is in the range 0·5–5%.

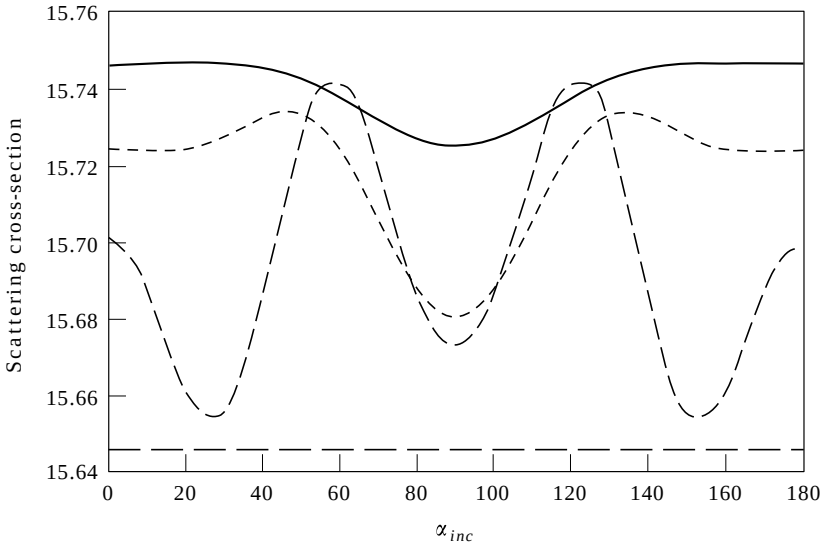

Figure 8. Fluidlike scatterer $k_e R = 5$ and $R_{cav} = 0{\cdot}05R$. ——, $D = 0{\cdot}0R$; ——, $D = 0{\cdot}4R$; ----, $D = 0{\cdot}6R$; – – – –, $D = 0{\cdot}8R$.

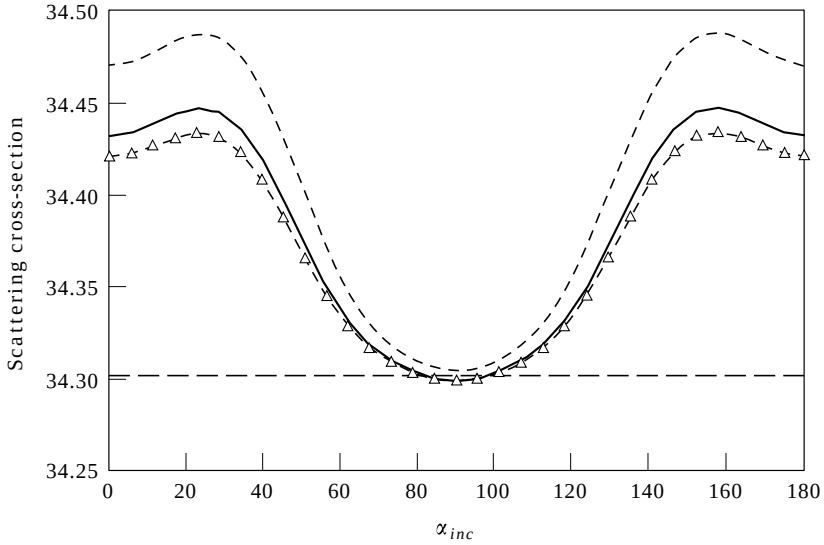

Figure 9. Fluidlike scatterer $k_eR = 10$ and $D = 0{\cdot}6R$. ——, $R_{cav} = 0{\cdot}0R$; – – – –, $R_{cav} = 0{\cdot}05R$; ——, $R_{cav} = 0{\cdot}01R$; –△–△–△–, $R_{cav} = 0{\cdot}005R$.

The behaviour of the scattering cross-section is influenced differently by the eccentricity of the cavity, for every dimensionless wave number. Whereas for $k_eR = 1$ the number of peaks is not modified by the position of the internal boundary, for $k_eR = 5$ and $k_eR = 10$, this number changes with D.

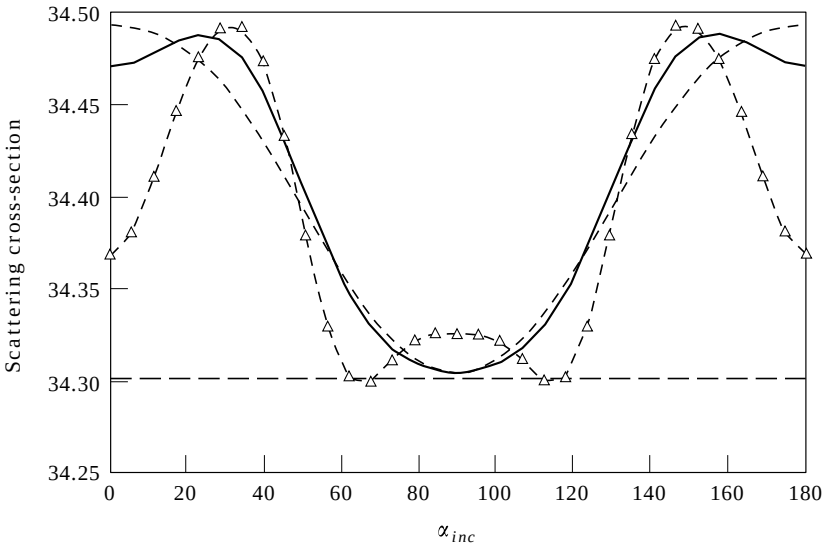

Figure 10. Fluidlike scatterer $k_eR = 10$ and $R_{cav} = 0{\cdot}05R$. ——, $D = 0{\cdot}0R$; – – – –, $D = 0{\cdot}4R$; ——, $D = 0{\cdot}6R$; –△–△–△–, $R_{cav} = 0{\cdot}8R$.

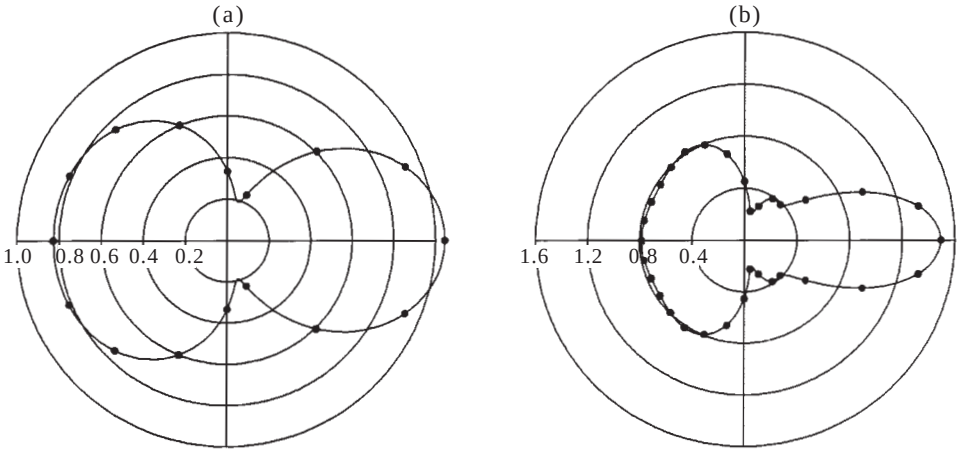

Figure 11. Angular distribution $|p_{sc}/p_{inc}|$ for brass in water with central cavity. Elastic scatterer; (a) $k_eR = 1$; (b) $k_eR = 3$. ——, Analytical solution; ●, BEM solution.

3. FLUID–SOLID SCATTERING

3.1. THE INTERACTION MODEL

In the case of an elastic obstacle, the external wave motion consists of the incident compressional wave and a scattered compressional wave, while the wave motion inside the scatterer includes a refracted compressional wave and a shear wave. This last part did not appear in the previous situation. In the linear steady state theory, the acoustic equation in the inviscid fluid is always represented by the Helmholtz equation, while the waves inside the scatterer can be described by the Cauchy–Navier equation. In the hypothesis of linear elasticity and the absence of body force, one has

$$\left(\frac{k_t^2}{k_l^2} - 1\right)\nabla(\nabla \cdot \mathbf{u}(\mathbf{x})) + \nabla^2\mathbf{u}(\mathbf{x}) + k_t^2\mathbf{u}(\mathbf{x}) = 0, \tag{9}$$

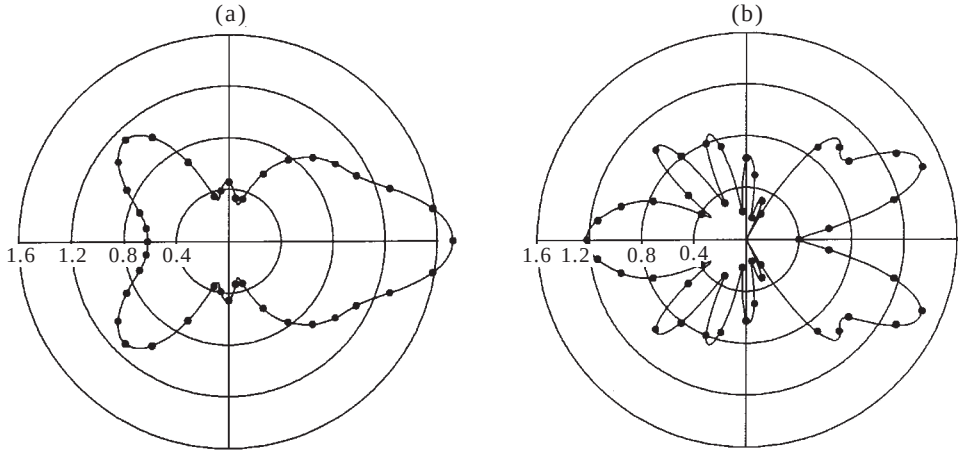

Figure 12. Angular distribution $|p_{sc}/p_{inc}|$ for brass in water with central cavity. Elastic scatterer; (a) $k_eR = 5$; (b) $k_eR = 10$. ——, Analytical solution; ●, BEM solution.

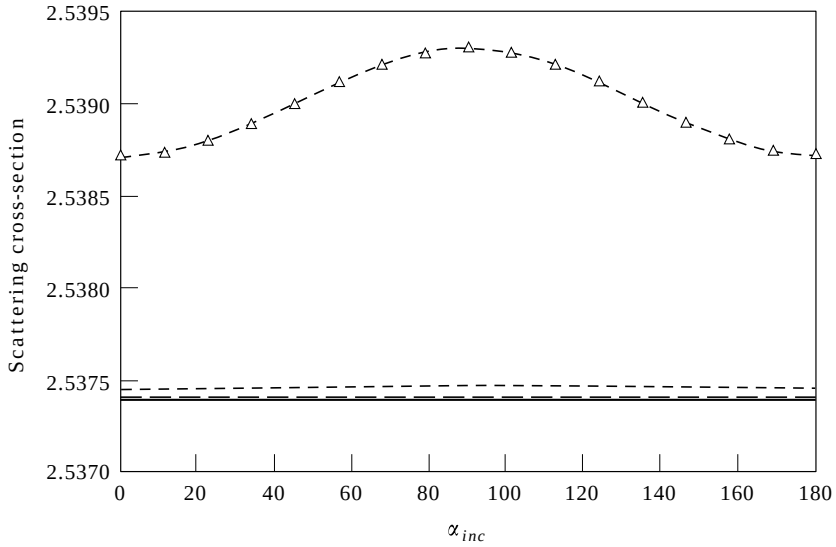

Figure 13. Elastic scatterer $k_e R = 1$ and $D = 0{\cdot}06R$. ——, $R_{cav} = 0{\cdot}0R$; –△–△–△–, $R_{cav} = 0{\cdot}05R$; – – – –, $R_{cav} = 0{\cdot}01R$; — —, $R_{cav} = 0{\cdot}005R$.

where k_l and k_t are the longitudinal and shear wave numbers in the solid, given by

$$k_l = \frac{\omega}{c_l}, \quad k_t = \frac{\omega}{c_t}, \quad c_l = \sqrt{\frac{\lambda + 2\mu}{\rho_i}} \quad c_t = \sqrt{\frac{\mu}{\rho_i}}.$$

The terms c_l and c_t are the longitudinal and transverse wave velocity, respectively, and λ, μ are the Lamé constants.

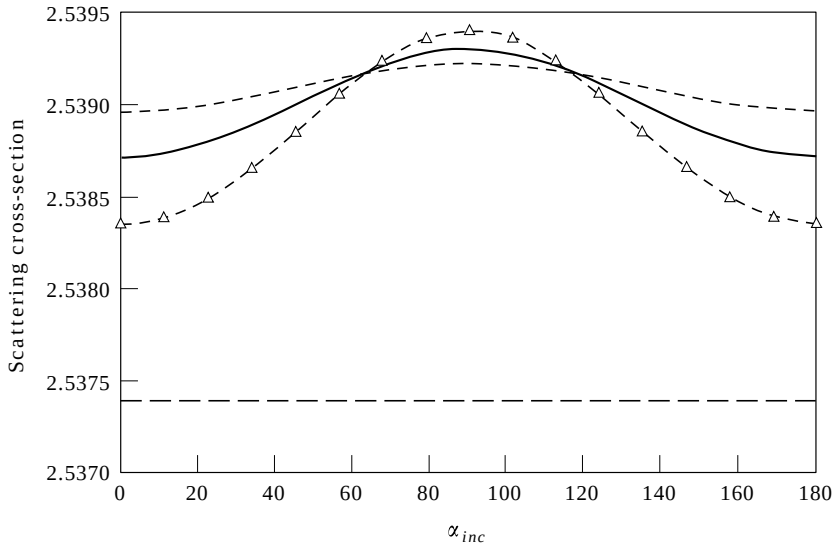

Figure 14. Elastic scatterer $k_e R = 1$ and $R_{cav} = 0{\cdot}05R$. — —, $D = 0{\cdot}0R$; – – – –, $D = 0{\cdot}4R$; ——, $D = 0{\cdot}6R$; –△–△–△–, $D = 0{\cdot}8R$.

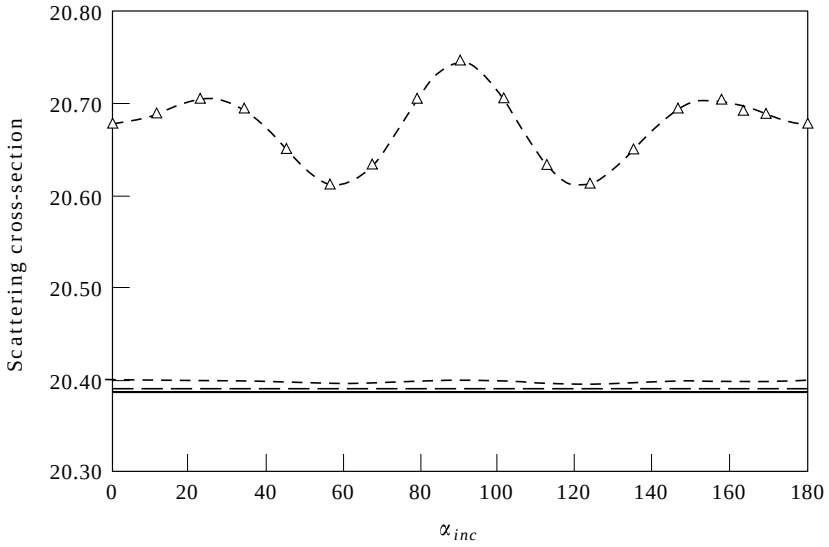

Figure 15. Elastic scatterer $k_e R = 5$ and $D = 0{\cdot}06R$. ——, $R_{cav} = 0{\cdot}0R$; –△–△–△–, $R_{cav} = 0{\cdot}05R$; ----, $R_{cav} = 0{\cdot}01R$; — —, $R_{cav} = 0{\cdot}005R$.

At the fluid–solid interface Γ_e, the pressures and fluxes p, q and the displacements and tractions $\mathbf{u}$, $\mathbf{t}$ satisfy the compatibility and equilibrium conditions, i.e., continuity of normal components of velocities and equilibrium of tractions

$$q(\mathbf{x}) = \rho_e \omega^2 \mathbf{u}(\mathbf{x}) \cdot \mathbf{n}(\mathbf{x}), \tag{10}$$

$$\mathbf{t}(\mathbf{x}) = -p(\mathbf{x})\mathbf{n}(\mathbf{x}),$$

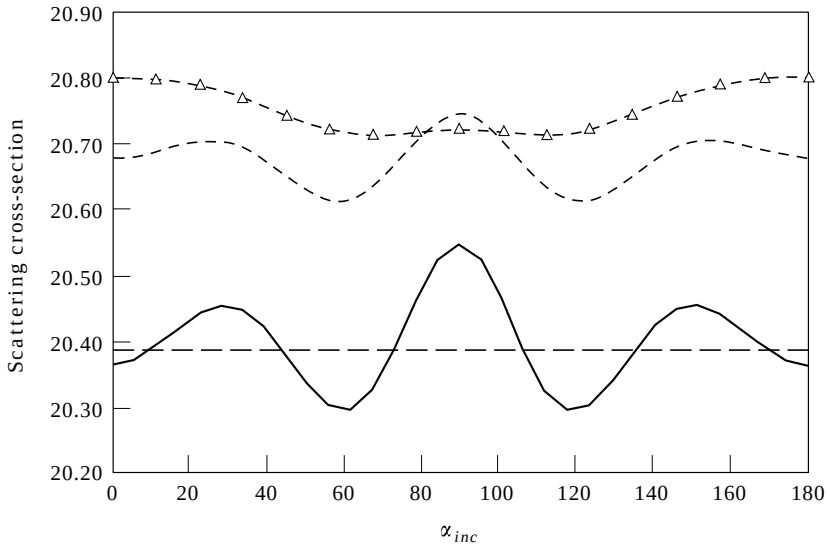

Figure 16. Elastic scatterer $k_e R = 5$ and $R_{cav} = 0{\cdot}05R$. — —, $D = 0{\cdot}0R$; –△–△–△–, $D = 0{\cdot}4R$; – – – –, $D = 0{\cdot}6R$; ——, $D = 0{\cdot}8R$.

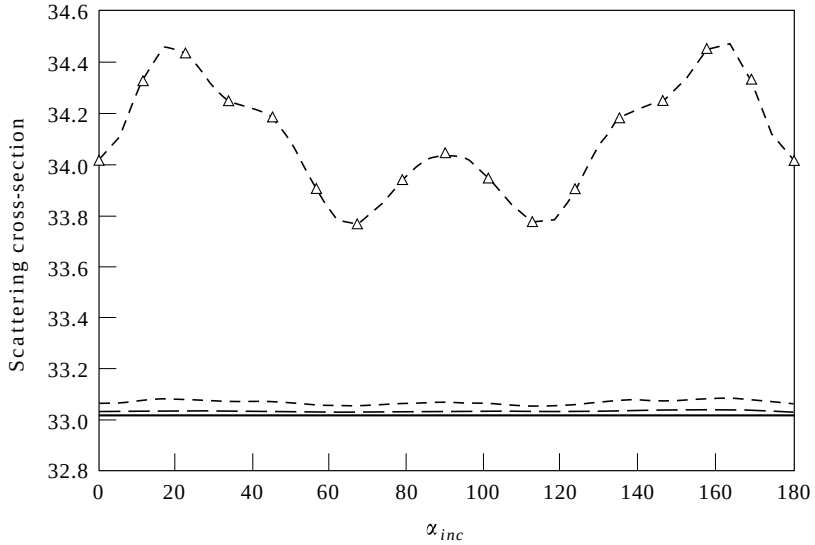

Figure 17. Elastic scatterer $k_e R = 10$ and $D = 0{\cdot}06R$. ——, $R_{cav} = 0{\cdot}0R$; –△–△–△–, $R_{cav} = 0{\cdot}05R$; – – – –, $R_{cav} = 0{\cdot}01R$; — —, $R_{cav} = 0{\cdot}005R$.

where **n** denotes the normal pointing inward into the solid, **u** and **t** are the elastic displacements and tractions, respectively.

The boundary integral equation corresponding to the governing equation (9) can be written as

$$c_{ij}(\boldsymbol{\xi})u_j(\boldsymbol{\xi}) + \int_{\Gamma} T_{ij}(\boldsymbol{\xi}, \mathbf{x})u_j(\mathbf{x})\, \mathrm{d}\Gamma(\mathbf{x}) = \int_{\Gamma} U_{ij}(\boldsymbol{\xi}, \mathbf{x})t_j(\mathbf{x})\, \mathrm{d}\Gamma(\mathbf{x}), \tag{11}$$

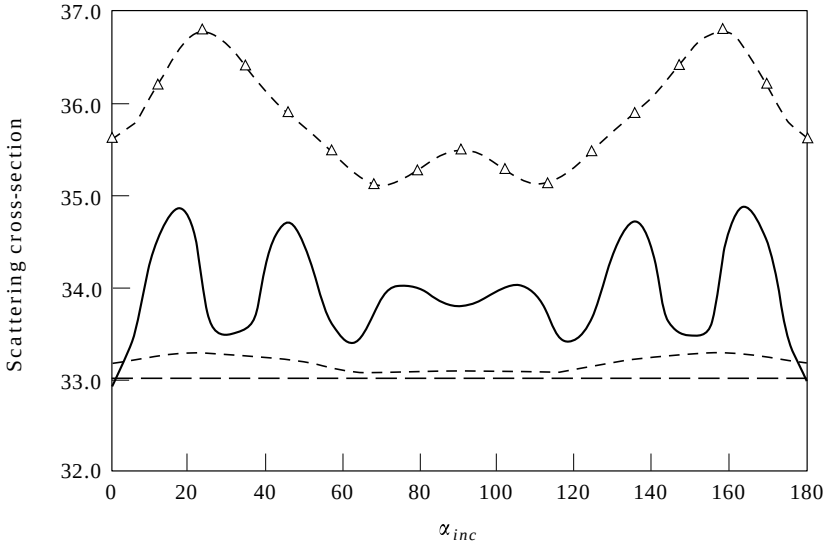

Figure 18. Elastic scatterer $k_e R = 10$ and $R_{cav} = 0{\cdot}05R$. — —, $D = 0{\cdot}0R$; – – – –, $D = 0{\cdot}4R$; –△–△–△–, $D = 0{\cdot}6$; ——, $D = 0{\cdot}8R$.

where $\oint$ stands for a Cauchy principal value integral, $T_{ij}(\boldsymbol{\xi}, \mathbf{x})$ and $U_{ij}(\boldsymbol{\xi}, \mathbf{x})$ are the fundamental solutions characterising response of an infinite elastic medium to a concentrated harmonic load of frequency ω. They are respectively displacements and tractions in the i direction for a unit harmonic load acting along the j direction.

In 2-D the expressions for $T_{ij}(\boldsymbol{\xi}, \mathbf{x})$ and $U_{ij}(\boldsymbol{\xi}, \mathbf{x})$ are the following

$$U_{ij} = \frac{1}{2\pi\rho_i c_t^2}\,[\psi\delta_{ij} - \chi r_{,i} r_{,j}],$$

$$T_{ij} = \frac{1}{2\pi}\left[\left(\psi_{,r} - \frac{1}{r}\,\chi\right)(\delta_{ij} r_{,n} + r_{,j} n_i)\right.$$

$$- \frac{2}{r}\,\chi(n_j r_{,i} - 2r_{,i} r_{,j} r_{,n}) - 2\chi_{,r} r_{,i} r_{,j} r_{,n}$$

$$\left. + \left(\frac{c_l^2}{c_t^2} - 2\right)\left(\psi_{,r} - \chi_{,r} - \frac{1}{r}\,\chi\right) r_{,i} n_{,j}\right].$$

The functions ψ and χ depend on the modified Bessel functions K_0, K_1 and K_2 and are given as

$$\psi = \mathrm{K}_0(\mathrm{i}k_t r) + \frac{1}{k_t r}\left[\mathrm{K}_1(\mathrm{i}k_t r) - \frac{c_t}{c_l}\,\mathrm{K}_1(\mathrm{i}k_l r)\right], \qquad \chi = \mathrm{K}_2(\mathrm{i}k_t r) - \frac{c_t^2}{c_l^2}\,\mathrm{K}_2(\mathrm{i}k_l r),$$

where $k_l = \omega/c_l$ and $k_t = \omega/c_t$. The kernels $U_{ij}(\boldsymbol{\xi}, \mathbf{x})$, $T_{ij}(\boldsymbol{\xi}, \mathbf{x})$ are $O(\ln r)$ and $O(1/r)$ singular, respectively.

The value of (2×2) matrix $c_{ij}(\boldsymbol{\xi})$ depends on the position of $\boldsymbol{\xi}$ and the smoothness of the boundary.

3.2. NUMERICAL IMPLEMENTATION

Displacements and tractions along the boundary are approximated with quadratic elements in the same way as for the scalar quantities (pressure and fluxes) described in the previous section.

The geometry of the element can also be considered as quadratic and represented by the nodal co-ordinates and the same interpolation functions $\phi_n(\zeta)$ used for the displacement and traction components.

The only difference between the present inplane discretisation process and that in the previous scalar problem is that the interpolation is now done independently for each component of the boundary displacement or traction, while in the fluid field only one component exists.

The discretised boundary integral equation at node $\bar{\boldsymbol{\xi}}$ can now be written as follows

$$c_{ij}(\bar{\boldsymbol{\xi}})u_j(\bar{\boldsymbol{\xi}}) + \sum_{l=1}^{EL}\sum_{n=1}^{3}\left\{\int_{-1}^{+1} T_{ij}(\bar{\boldsymbol{\xi}}, \mathbf{x}(\zeta))\phi_n(\zeta)\mathrm{J}_l(\zeta)\,\mathrm{d}\zeta\right\}u_j^n$$

$$= \sum_{l=1}^{EL}\sum_{n=1}^{3}\left\{\int_{-1}^{+1} U_{ij}(\bar{\boldsymbol{\xi}}, \mathbf{x}(\zeta))\phi_n(\zeta)\mathrm{J}_l(\zeta)\,\mathrm{d}\zeta\right\}t_j^n. \tag{12}$$

The same Gaussian numerical procedure as in the previous section can be used to calculate the integral on every boundary element.

Equation (7a) applied on Γ_e and equation (12) applied on Γ represent the uncoupled system of $3NB + 2NC$ equations with the $4NB$ unknown pressures, fluxes and components of tractions on Γ_e and $2NB + 2NC$ components of displacements on Γ. They can be written in matrix form as

$$\mathbf{H}^e\mathbf{p} - \mathbf{G}^e\mathbf{q} = \mathbf{p}_{inc},$$
$$\mathbf{H}^i\mathbf{u} - \mathbf{G}^i\mathbf{t} = \mathbf{0}. \tag{13}$$

The vectors $\mathbf{p}$, $\mathbf{q}$ and $\mathbf{u}$, $\mathbf{t}$ contain the external pressures, fluxes and, the internal displacements and tractions, respectively.

NB denotes the number of nodes on Γ_e and NC the number of nodes on Γ_i. The final algebraic set of equations is obtained adding the boundary conditions (10) on Γ_e, with the further condition $\mathbf{t} = 0$ on Γ_i and dividing the whole boundary into three-noded quadratic isoparametric elements:

$$\begin{bmatrix} \mathbf{H}^e & \mathbf{0} & \mathbf{0} & -\mathbf{G}^e & \mathbf{0} \\ \mathbf{0} & \mathbf{H}^i_{\Gamma_e\Gamma_e} & \mathbf{H}^i_{\Gamma_e\Gamma_i} & \mathbf{0} & -\mathbf{G}^i_{\Gamma_e\Gamma_e} \\ \mathbf{0} & \mathbf{H}^i_{\Gamma_i\Gamma_e} & \mathbf{H}^i_{\Gamma_i\Gamma_i} & \mathbf{0} & -\mathbf{G}^i_{\Gamma_i\Gamma_e} \\ \mathbf{0} & \rho_e\omega^2 N^t & \mathbf{0} & -\mathbf{I} & \mathbf{0} \\ \mathbf{N} & \mathbf{0} & \mathbf{0} & \mathbf{0} & \mathbf{I} \end{bmatrix} \begin{Bmatrix} \mathbf{p} \\ \mathbf{u}_{\Gamma_e} \\ \mathbf{u}_{\Gamma_i} \\ \mathbf{q} \\ \mathbf{t}_{\Gamma_e} \end{Bmatrix} = \begin{Bmatrix} \mathbf{p}_{inc} \\ \mathbf{0} \\ \mathbf{0} \\ \mathbf{0} \\ \mathbf{0} \end{Bmatrix}.$$

The submatrix N collects the components of the inward normals on Γ_e, and $\mathbf{I}$ is the identity matrix.

The final matrix is more ill-conditioned than the previous problem whenever material parameters are used. Such a combination is sometimes referred to as weakly coupled since it represents the merger of two physically different sets of equations. The fact that the interface continuity provides coupling only in the normal direction could contribute to this weak coupling.

The solution of the combined system has therefore to incorporate appropriate scaling and use at least double precision computation.

The integration process is analogous to that used in the previous scalar problem. The fundamental solutions are decomposed into their static and dynamic parts, to isolate the singularity. $\mathbf{H}^i$ and $\mathbf{G}^i$ are calculated by Gaussian quadrature with 16 points when the source point does not belong to the integration element. The

diagonal term of the $\mathbf{H}^i$ matirx is evaluated together with the $c_{ij}(\bar{\boldsymbol{\xi}})$ coefficient by applying the static rigid body condition (keeping in mind that the singularity of the dynamic fundamental solution is the same as that of the static one). The singular term of the $\mathbf{G}$ matrix can be evaluated using the same procedure as the previous problem; the only difference is that the kernel to be integrated has some more terms than in the scalar problem.

3.3. NUMERICAL EXAMPLES

In the examples presented here, the dimensions and properties of fluid and scatterer are the same as the previous scalar problem. The elastic scatterer has cylindrical shape and is immersed in an infinite fluid carrying an incoming incident wave. The properties of the fluid and solid are given in Table 1.

In order to check the accuracy of the coupled elastic solid–fluid BEM formulation, some test examples are considered for which analytical solutions are available. Figures 11 and 12 compare the analytical and boundary element farfield coefficients in the cases $k_e R = 1, 3, 5, 10$.

For this problem, an analytical solution can be obtained in the presence of a central cavity. Following reference [30], but modifying the compressive and transverse waves inside the solid, we have

$$\mathbf{u} = \nabla\phi + \nabla \times \boldsymbol{\psi},$$

$$\phi = \sum_{m=0}^{\infty} \varepsilon_m i^m a_m \mathrm{J}_m(k_1 r)\cos(m\theta) + \sum_{m=0}^{\infty} \varepsilon_m i^m c_m \mathrm{H}_m(k_1 r)\cos(m\theta),$$

$$\boldsymbol{\psi} = \sum_{m=0}^{\infty} \varepsilon_m i^m b_m \mathrm{J}_m(k_2 r)\sin(m\theta) + \sum_{m=0}^{\infty} \varepsilon_m i^m d_m \mathrm{H}_m(k_2 r)\sin(m\theta).$$

It is possible to obtain the scattering pressure on the external circle as the sum of a series in which the mth term involves the resolution of a 5×5 (and not 3×3) system of linear equations: the matrix coefficients are in terms of the Bessel functions of the first and third kind, of order m.

The first 25 terms of the series solution and 20 terms of the Bessel function expansions were taken into account in order to obtain a satisfactory stable analytical solution.

The examples show that there is good agreement between the boundary element method and the analytical solution. In the case $k_e R = 1$, $8 + 8$ elements on $\Gamma_e \cup \Gamma_i$ are enough to obtain a numerical solution with an error smaller than 1%, while $16 + 8$, $20 + 8$ and $28 + 8$ elements are necessary to obtain the same precision in the cases $k_e R = 3, 5, 10$. The increasing number of elements is due to an increased variation in the solution requiring finer meshes.

The comparison between Figures 3(a), 11(a) and between Figures 4(a), 12(b) show the difference of behaviour in the scattered response on the external circle of the two modes respectively for $k_e R = 1$ and $k_e R = 10$.

In Figures 13–18 the scattering cross-section is diagrammed versus the incident angle for $k_e R = 1, 5, 10$ and for different sizes and positions of the internal cavity.

For all the wave numbers considered, the results show a lower sensitivity compared to the results of fluid–fluidlike scatterer, both with respect to the size and the position of the internal cavity.

In the case $k_e R = 1$, it appears from Figure 13 that the difference, in scattering cross-section, between the solid without the cavity and with the cavity becomes too small (0·01%) when the size of the cavity is 1–0·5% of the cylinder's size.

In the cases $k_e R = 5, 10$, as expected, the sensitivity is higher and the above value is of a order 1–5%.

The same behaviour is noticed with respect to the position of the cavity, but the minimum difference in scattering cross-section reaches higher values (0·1–0·2% for $k_e R = 1$ and up to 10% in the other cases).

The sensitivity could be improved by amplifying the incident pressure; the examples shown, in fact, all refer to an incident acoustic amplitude of 60 dB.

4. CONCLUSIONS

The application of the boundary element method to two different coupled problems for the analysis of the interaction of a plane sound wave with a cylinder immersed in an inviscid fluid was presented. An internal boundary was considered inside the scatterer.

In the first part, the cylinder was modelled by the Helmholtz equation, i.e., it was supposed not to be able to support shear waves, while in the second part, the Navier–Cauchy equation was used to describe the obstacle. In both models, continuity of the normal components of velocities and equilibrium of the tractions were enforced at the interface between the two fields. The method was shown to be accurate for both problems.

Numerical examples were given for different sizes and positions of the internal boundary. In both models, the method was able to characterize the internal cavity by measurements for different incident angles.

The solution was shown to be more sensitive in the case in which the scatterer was unable to support shear waves. The differences are essentially due to the different physical models used to describe the scatterer: the elastic field is more rigid and therefore less *influenced* by the load represented by the incident wave.

REFERENCES

1. A. C. Cangellaris and R. Lee 1991 *IEEE Transactions on Antennas and Propagation* **39**, 645–650. Finite element analysis of electromagnetic scattering from inhomogeneous cylinders at oblique incidence.
2. G. Pelosi, R. Coccioli and R. D. Graglia 1994 *Journal of Physics D*: *Applied Physics* **27**, 2013–2018. A finite-element analysis of electromagnetic scattering from a moving dielectric cylinder of arbitrary cross section.
3. A. Khebir, J. D'Angelo and J. Joseph 1993 *IEEE Transactions on Antennas and Propagation* **41**, 534–541. A new finite element formulation for RF scattering by complex bodies of revolution.

4. H. Gan, P. L. Levin and R. Ludwig 1993 *Journal of Acoustic Society of America* **94**, Pt. 1, 1651–1662. Finite element formulation of acoustic scattering phenomena with absorbing boundary condition in the frequency domain.
5. A. Kirsch and P. Monk 1994 *IMA Journal of Numerical Analysis* **14**, 523–544. An analysis of the coupling of finite-element and Nystrom methods in acoustic scattering.
6. J. D. Collins, J. L. Volakis and J. M. Jin 1990 *IEEE Transactions on Antennas and Propagation* **38**, 1852–1858. A combined finite element-boundary integral formulation for solution of two-dimensional scattering problems via CGFFT.
7. J. M. Jin, J. L. Volakis and J. D. Collins 1991 *IEEE Antennas and Propagation Magazine* **33**, 22–32. A finite-element–boundary-integral method for scattering and radiation by two- and three-dimensional structures.
8. B. Dubus 1994 *Journal of Acoustic Society of America* **96**, 3792–3799. Coupling finite element and boundary element methods on a mixed solid–fluid/fluid–fluid boundary for radiation or scattering problems.
9. A. F. Seybert, C. Y. R. Cheng and T. W. Wu 1990 *Journal of Acoustic Society of America* **88**, 1612–1618. The solution of coupled interior/exterior acoustic problems using boundary element method.
10. M. C. Au and C. A. Brebbia 1983 *Applied Mathematical Modelling* **7**, 106–114. Diffraction of water waves for vertical cylinders using boundary elements.
11. S. Shenoy, T. J. Rudolphi and F. J. Rizzo 1995 in *Boundary Elements XVII* (C. A. Brebbia, S. Kim, T. A. Osswald and H. Power, editors) 502–512. Computational Mechanics Publications, Southampton. Boundary element solutions to wave scattering by surface irregularities on a fluid–solid interface.
12. T . Terai 1980 *Journal of Sound and Vibration* **69**, 71–100. On calculation of sound fields around three dimensional objects by integral equation methods.
13. W. S. Hall and W. H. Robertson 1988 in *Boundary Elements X*, vol. 4 (C. A. Brebbia, editor) 301–315. Berlin: CMP/Springer-Verlag. Boundary element methods for acoustic wave scattering.
14. C. Jin 1993 *Engineering Analysis with Boundary Elements* **12**, 39–46. A direct boundary integral equation method for the acoustic scattering problem.
15. M. A. Jaswon and S. I. Zaman 1993 in *Boundary Elements XV*, vol. 1 (C. A. Brebbia and J. J. Rencis, editors) 281–303. Amsterdam: CMP/Elsevier Science Publishers. A new BEM formulation of acoustic scattering problems.
16. H. A. El-Mirati and J. B. Davies 1987 *IEEE Transactions on Antennas and Propagation AP*-**35**, 539–544. Improved boundary element techniques for two-dimensional scattering problems with circular boundaries.
17. A. F. Seybert, B. Soenarko, F. J. Rizzo and D. J. Shippy 1986 *Journal of Acoustic Society of America* **80**, 1241–1247. A special integral equation formulation for acoustic radiation and scattering for axisymmetric bodies and boundary conditions.
18. A. F. Seybert and D. K. Casey 1988 *Journal of Acoustical Society of America* **84**, 379–384. An integral equation method for coupled fluid/fluid scattering in three-dimensions.
19. A. F. Seybert, T. W. Wu and X. F. Wu 1988 *Journal of Acoustical Society of America* **84**, 1906–1912. Radiation and scattering of acoustic waves from elastic solids and shells using the boundary element method.
20. P. P. Goswami, T. J. Rudolphi, F. J. Rizzo and D. J. Shippy 1990 *Journal of Nondestructive Evaluation* **9**, 101–112. A boundary element model for acoustic-elastic interaction with applications in ultrasonic NDE.
21. A. D. Pierce 1981 *Acoustics*: *An Introduction to its Physical Principles and Applications* (F. J. Cerre and M. Eichberg, editors) 177–178. New York: McGraw-Hill Book Company.
22. H. A. Schenck 1968 *Journal of Acoustical Society of America* **44**, 41–58. Improved Integral formulation for acoustic radiation problems.

23. A. J. Burton and G. F. Miller 1971 *Proceedings Royal Society London A* **323**, 201–210. The application of integral equation methods to the numerical solution of some exterior boundary value problems.
24. W. L. Meyer, W. A. Bell, B. T. Zinn and M. P. Stallybrass 1978 *Journal of Sound and Vibration* **59**, 245–262. Boundary integral solutions of three dimensional acoustic radiation problems.
25. M. Abramowitz and I. A. Stegun 1964 *Handbook of Mathematical Functions* (M. Abramowitz and I. Stegun, editors) 358–389. New York: Dover Publications Inc.
26. M. H. Aliabadi, W. S. Hall and T. G. Phemister 1985 *International Journal for Numerical Methods in Engineering* **21**, 2221–2236. Taylor expansions for singular kernels in the boundary element method.
27. J. Dominguez 1993 *Boundary Elements in Dynamics*. Computational Mechanics Publications, Southampton.
28. J. A. Roumeliotis and N. B. Kakogiannos 1995 *Journal of Acoustical Society of America* **97**, 2074–2081. Acoustic scattering from an infinite cylinder of small radius coated by a penetrable one.
29. D. S. Jones 1986 *Acoustic and Electromagnetic Waves*. Oxford: Clarendon Press. See pp. 414–416.
30. W. H. Lin and A. C. Raptis 1983 *Journal of Acoustical Society of America* **73**, 736–748. Acoustic scattering by elastic solid cylinders and spheres in viscous fluids.